



CHORUS

This is the accepted manuscript made available via CHORUS. The article has been published as:

Vortex cutting in superconductors

A. Glatz, V. K. Vlasko-Vlasov, W. K. Kwok, and G. W. Crabtree

Phys. Rev. B **94**, 064505 — Published 9 August 2016

DOI: [10.1103/PhysRevB.94.064505](https://doi.org/10.1103/PhysRevB.94.064505)

Vortex cutting in superconductors

A. Glatz^{1,2}, V. K. Vlasko-Vlasov¹, W. K. Kwok¹, G. W. Crabtree^{1,3}

¹*Materials Science Division, Argonne National Laboratory, Argonne, Illinois 60439, USA*

²*Department of Physics, Northern Illinois University, DeKalb, IL 60115 USA*

³*Department of Physics, University of Illinois at Chicago, Chicago, IL 60607 USA*

Abstract

Vortex cutting and reconnection is an intriguing and still-unsolved problem central to many areas of classical and quantum physics, including hydrodynamics, astrophysics, and superconductivity. Here we describe a comprehensive investigation of the crossing of magnetic vortices in superconductors using time dependent Ginsburg-Landau modeling. Within a macroscopic volume we simulate initial magnetization of an anisotropic high temperature superconductor followed by subsequent remagnetization with perpendicular magnetic fields, creating the crossing of the initial and newly generated vortices. The time resolved evolution of vortex lines as they approach each other, contort, locally conjoin and detach, elucidates the fine details of the vortex-crossing scenario under practical situations with many interacting vortices in the presence of weak pinning. Our simulations also reveal left-handed helical vortex instabilities that accompany the remagnetization process and participate in the vortex crossing events.

Introduction

Magnetic field lines introduced by Michael Faraday nearly two centuries ago are a very useful abstraction that represents the behavior of magnetic fields [1]. They provide a visual picture of the magnitude and direction of magnetic fields in vacuum, in magnetic media and at their boundaries. In reality, the presentation of the continuous magnetic fields by a set of discrete field lines is just a convenient construction. These *imaginary magnetic field lines* can be straight or curved, converge into dense contours that portray enhanced fields or diverge into sparse arrays for decreased fields, but they *neither cross nor entangle*.

In contrast, in a type-II superconductor below the superconducting transition temperature, the magnetic field actually enters in the shape of separate flux lines - *real material elastic strings* - Abrikosov vortices comprised of supercurrents circulating around a normal core that can carry one or more (in mesoscopic samples) magnetic flux quanta ($\Phi_0 = h/2e$) [2-4]. The normal core of vortices has the characteristic size of the coherence length (ξ) and the surrounding circulating supercurrents decay at the distance of the London penetration depth $\lambda \gg \xi$. These vortices are the principal building blocks for complex matter-like assemblies, as they form lattices and melt into a liquid state with thermal fluctuations. The statics and dynamics of 'vortex matter' depend on their many interactions, with surfaces, defects in the crystal structure, applied transport currents, and with each other. Vortices and their interactions define the basic electromagnetic response of superconductors and hence their fundamental understanding is crucial for fundamental science and for applications in superconducting power lines, high-field magnets, microwave filters [5-7] and potential quantum computer circuits [8, 9].

Unlike Faraday's abstract magnetic field lines, vortices in a superconductor *can cross, cut, and reconnect or entangle* with each other in complex dynamic processes that currently lack a clear theoretical description. Although long-range repulsion of vortices resists their close approach, suitable combinations of thermal fluctuations, pinning and driving forces may bring two flexible vortex lines together to cross, cut and reconnect or entangle in complex topologies.

One can imagine different outcomes when vortices approach each other. The repulsive energy at the point of closest approach may be too large to be overcome, preventing vortices from touching, cutting or penetrating through each other. In this case, further vortex motion elsewhere along their lengths could bring the vortices close to other neighboring vortices and create a topologically entangled configuration, such as an orderly braid of several vortices or a randomly entangled "bowl of spaghetti." On the other hand, if the repulsive barrier is sufficiently small, the vortices may penetrate each other, preventing the formation of an entangled state. At the point of local contact, instead of merely crossing through each other, two vortices could exchange vortex halves on either side of the point of contact producing a new reconnected configuration.

Vortex crossing and reconnection are often invoked in treating the dynamics of dense vortex systems such as pinned vortex liquids and entangled vortex solids, particularly in high temperature superconductors where thermal energies enable a larger degree of vortex motion [10-13]. Beyond superconductivity, vortex crossing is a general physical phenomenon actively discussed in the dynamics of classical and quantum liquids including astrophysical plasmas and atomic Bose-condensates [14-17].

In this paper, we present time dependent Ginzburg-Landau simulations of arrays of vortices in a finite-sized sample that is initially magnetized in one direction and then re-magnetized with an orthogonal magnetic field. In this process, vortices created by the orthogonal remagnetization field come in contact with the initially generated vortices allowing vortices with different orientations to touch, penetrate, or cut and reconnect. The simulations use material parameters typical of $\text{YBa}_2\text{Cu}_3\text{O}_{7-d}$ (YBCO) high temperature superconductors. Our simulations reveal a complex mechanism for vortex cutting: when two vortices approach, at the nearest point they locally bend so that the polarity of bent segments becomes opposite, converting their local mutual repulsion to local mutual attraction. The vortices then merge at the point of closest approach and re-emerge as independent vortices having exchanged their respective half-vortices. After cutting, reconnecting and straightening, the new vortices tilt towards the applied field direction, resulting in the rotation of the magnetic flux inside the superconductor.

Background

Despite the pervasiveness of vortex crossing in many physical systems, the fundamental description of the phenomenon remains a challenge. It has been discussed theoretically in various contexts, often with simplifying assumptions to make theoretical analysis tractable. The easiest simplification is to focus on the interactions of two vortices [18] removed from the interactions with the surrounding vortices

Oftentimes the analysis is carried out considering the separate contributions to the total vortex energy, such as the long-range magnetic repulsion due to interacting circulating supercurrents, the short-range attraction due to overlapping normal vortex cores and the elastic energy due to local vortex bending. Even with these simplifying assumptions, the analysis is challenging because these energies depend locally on each other, making them difficult to identify and treat independently.

The dependence of vortex interaction on the angle between them adds a fascinating and complicating feature: as two vortices approach, they can replace their mutual repulsion at the point of closest approach with mutual attraction if they bend sufficiently to point locally in opposite directions. In this case, the elastic energy of bending, the attractive or repulsive energy of interacting circulating supercurrents and the condensation energy of the normal core are intimately connected and cannot be readily separated. In the presence of such extreme local distortions, the *neighboring* vortices will deform significantly as well and their energy of local deformation must be included. Moreover, at close distances the current patterns near crossing vortices transform so strongly that the concept of individual flux lines becomes irrelevant and an accurate account of the complete current pattern needs to be taken into account.

Vortex cutting still lacks even a qualitative coherent description [19], although many of the general physical effects involved in the process were clarified earlier by Brandt et al. [18]. At close enough distances, straight rigid crossing vortex cores experience an attractive interaction, due to the reduction of the total normal core volume by $\sim \xi^3$ (assuming that the length of the overlap as $\sim \xi$). However, to come close enough for this to happen, vortices must overcome strong electromagnetic repulsion due to the circulating supercurrents surrounding the vortices over the penetration depth distance, $r \sim \lambda$. The repulsive force reaches a maximum at short distances $\geq \xi$, where the strong λ -range repulsion changes to

the weak, short-range attraction. Initially, it was suggested that the value of this maximum, characterizing the activation barrier of the vortex crossing, U_x , is extremely high (see refs. in [18]). However, calculations of the crossing energy of straight rigid vortices in [18] demonstrated that it can have a reasonably moderate value. It was clearly shown that the flux cutting potential is dominated by electromagnetic interactions, while the contribution due to the vortex core overlap is small. U_x drops with decreasing Ginzburg-Landau parameter $\kappa=\lambda/\xi$, which corresponds to the decreasing role of λ -repulsion and increasing contribution of ξ -attraction. For larger angles between straight flux lines, the crossing barrier becomes smaller and for vortices tilted by more than 90 degrees, the interactions become attractive at all distances. At the boundary value of $\kappa\sim(1/2)^{1/2}$, corresponding to the transition from type-II to type-I superconductivity, and for any angles between vortices, their interactions become attractive, as was confirmed by observations of coupled vortex domains in pure niobium samples [20-21].

Further account of the local bending of *flexible* vortex lines near the contact point where the vortices re-align into antiparallel configurations to reduce their mutual repulsion, revealed that the expected value of U_x can be noticeably smaller than for straight vortices [22]. A decrease of the vortex crossing energy in spite of the increase in the self-energy due to the increased length of bending, revealed that crossing of straight rigid vortices is hardly a proper description. In fact, estimates of the cutting barrier for straight non-parallel vortices yield very large barrier, $U_x\sim 50k_B T_c$, which would prevent vortex crossing (e.g. [10]).

Later, the effect of bending of the crossing vortices was calculated for anisotropic SCs with different penetration depth along different directions (e.g. $\Gamma=\lambda_c/\lambda_{ab} \sim 5$ in YBCO) [23]. In this case, the shape of vortex bending is determined by the anisotropy of the vortex line tension. Interestingly, the line tension or rigidity of vortices is maximum for orientations with minimum vortex line energy and U_x increases relative to the isotropic case. In contrast, in [24] it was found that for moderate Ginzburg-Landau parameters ($\kappa=\lambda/\xi \sim 10$) and not very large fields, the cutting energy should decrease with anisotropy as $\sim 1/\Gamma$. Calculations of the crossing barrier were also performed for anisotropic materials in the high-field limit ($H\sim H_{c2}$) [25, 12]. In high fields, the crossing vortices cannot be considered separately from the rest of the vortex matter, but still a noticeable U_x of the order of a few $k_B T_c$ was reported. Thus the value of the crossing barrier and consequently the probability of vortex cutting remains poorly defined. The effects of vortex rigidity, dependence on the Ginzburg-Landau parameter, and the role of anisotropy are important factors defining the crossing process, which still awaits a proper description.

A crucial point of the vortex-crossing phenomenon, which requires special attention and still remains an open question, is the local collapse of the vortex lines. Apparently even a long parallel vortex and antivortex will initially collapse at a single point and then the resulting U-shaped vortex arcs will shrink in opposite directions until they disappear. How the current patterns around the cores of colliding vortices transform in time and space during close approach and intersection of vortex centers is not obvious. In fact, between vortices, which are strongly bent around the crossing point to create the vortex-antivortex configuration, supercurrents should be strongly enhanced upon the mutual approach of the

vortex lines. Eventually they should go through an abrupt topological change when the cores of vortices merge. So far, this scenario, which also emerges when vortex and antivortex collapse in classical and quantum liquids, has not been clarified theoretically. We found the only illustration of the current distributions around close 2D vortex-antivortex pairs in [26] and with a lower resolution in [27].

Perhaps the most spectacular description of the crossing process was obtained by time dependent Ginzburg-Landau simulations in [28]. There, it was shown that two colliding perpendicular vortices first locally bend, cut, and reconnect, exchanging vortex halves. Subsequently, reconnected vortices cross and cut again, exchange their halves back and reconnect into the original vortices, which eventually diverge from each other. Such a striking double-step process requires special conditions that preserve the motion of the vortex tails and recover the original vortices after collapse. It was pointed out in [28] that in the presence of other vortices, the crossing process could be different. Hence the picture of two individual crossing vortices, although important for understanding the cutting/reconnection process, is oversimplified, as it neglects interactions with neighboring vortices and coupling of vortices to external fields.

Time Dependent Ginzburg-Landau Simulations

In this work we clarify the flux-cutting scenario using large scale TDGL simulations on a sample containing an array of longitudinal vortices, remagnetized by a perpendicular field. The model parameters were chosen close to those of modern anisotropic high- T_c superconductors and at magnetic fields high enough to produce multiple vortices in the simulation volume. We reveal specific features of the flux evolution for an ensemble of vortices generated by one direction of the applied magnetic field (longitudinal $H_{||}$) under steadily increasing perpendicular magnetic field (H_{\perp}). Successive images of the flux patterns show that new entering vortices with perpendicular field component, cut initial longitudinal vortices in a single stage process after an almost 180° local twist. The shape of this twist is distinctively controlled by the anisotropy. The crossing event occurs as an instantaneous collapse of the antiparallel segments, leaving local bends on the reconnected vortices. The resulting new vortices – consisting of the halves of initial vortices – straighten and tilt with respect to their pre-collision orientation. This process rotates the flux towards the applied field direction in the bulk of the superconductor upon progressive entry of new flux components from the sample edges. Accompanying this process is a helical vortex instability [29, 30] induced by currents screening the perpendicular field and flowing parallel to the initial vortices (see details in the last section) Expanding left-handed vortex helices cross longitudinal flux lines and also result in a tilt of vortices towards the applied field. Some results of our early simulations are presented in [31].

Model

To study vortex dynamics in crossing magnetic fields we use a recently introduced large-scale solver for time-dependent Ginzburg-Landau equations allowing visualization of dynamics of mesoscopically large vortex arrays within relatively large spatial volumes [32]. It relies on the numerical integration of the TDGL in the large- λ limit using graphics card processing units (GPUs).

The TDGL model was first suggested by Schmid in a very clever attempt to describe the relaxation in the Ginzburg-Landau equilibrium state by adopting the kinetic description of liquid helium by Landau-Khalatnikov [33]. Later, Gorkov and Eliashberg presented a microscopic derivation of TDGL [34]. In spite of limited formal range of applicability ($T \sim T_c$, [34-35]), so far TDGL is the most relevant and widely used approximation for modeling the flux dynamics in superconductors (see e.g. [36-41] and refs there. Although the TDGL model has a confirmed applicability only in the gapless superconductors [35], it is believed to provide a reasonable approach to analyze the vortex dynamics. In this work we use the dimensionless form of the TDGL equation for the complex superconducting order parameter ψ , which reads [32]:

$$\partial_t \psi + i\mu\psi = \varepsilon(r)\psi - |\psi|^2\psi + \left[\underline{g}(\nabla - i\mathbf{A}) \right]^2 \psi + \zeta(\mathbf{r}, t) \quad (1)$$

Here μ is the scalar potential calculated self-consistently from the Poisson equation, \underline{g} is the anisotropy tensor, and \mathbf{A} is the vector potential. Compared to the traditional TDGL form, (1) includes anisotropy through the anisotropy tensor \underline{g} . The equation also accounts for weak disorder, represented by the function $\varepsilon(r)$, and thermal noise $\zeta(\mathbf{r}, t)$. To model HTS we use parameters characteristic for YBCO. The length is scaled in units of zero-temperature coherence length $\xi_0 = \xi_{ab}$, the unit of time is the Ginzburg-Landau time $\tau_{GL} = \pi\hbar/8k_B T_c$, and the magnetic field is scaled to $B_{c2}(T=0) = \Phi_0/2\pi\xi_0^2$. Quenched disorder imitating the weak pinning is described by modulations of the critical temperature in the simulation volume with random function $\varepsilon(r) = \frac{T_c(r)}{T} - 1$ changing in the interval [0.8,1] yielding 10% variations of T_c . For YBCO, the anisotropy rescales the gauge-invariant gradient along the z-axis ($|\mathbf{c}|$) by a factor of $g=5$. In this case we neglect the layered crystal structure of the sample and account only for the mass anisotropy ($g=(m_c/m_{ab})^{1/2}$). The vector potential is taken as $\mathbf{A} = y[-B_z, 0, B_x]^T$. And the thermal noise is defined by spatio-temporal correlator $\langle \zeta(\mathbf{r}, t)\zeta(\mathbf{r}', t') \rangle \propto \frac{T}{T_c} \delta(\mathbf{r} - \mathbf{r}')\delta(t - t')$ where we choose $T=T_c/2$. We do not account for the magnetization currents defining the reduced magnetic induction in the superconductor compared to the applied magnetic field. However, such a simplification is relevant in the range of relatively large fields used in simulations. The equation is discretized on a regular spatial mesh of 256x256x128 grid points with $\xi_0/2$ unit step. In such a volume, we could realistically capture the dynamics of many interacting vortices with $0.1\tau_{GL}$ time resolution within a reasonable calculation time. A typical simulation run integrates 10^6 time steps and takes 3×10^4 s real time on a K20x NVidia tesla GPU. By choosing the minimum discretization mesh of $\xi_0/2$ we keep in mind that the Ginzburg-Landau theory is phenomenological in nature and describes physical properties on the scale larger than the superconducting coherence length. The time integration in our TDGL simulations is done using an implicit Crank-Nicolson scheme [ref JCOMP], which is stable for arbitrary time discretization. So, $0.1\tau_{GL}$ time resolution assures physically relevant dynamic behavior of the order parameter.

To understand the effect of disorder imitating weak pinning in the system, we compare calculations with results at $\varepsilon(r)=1$ (no spatial disorder, but only thermal noise present). We model two different geometries to address the shape effect relevant for thin crystal plates of high- T_c superconductors. One of them corresponds to the anisotropic plate

with surfaces parallel to the anisotropy axis \mathbf{c} . Another corresponding to cuprate crystals mimics a plate perpendicular to the \mathbf{c} -axis. Boundary conditions are open at the sample surfaces ($\parallel \mathbf{c}$ and $\perp \mathbf{c}$, respectively, for above geometries) and quasi-periodic in the other two directions. At open boundaries, the perpendicular supercurrent components are set to zero, while at quasi-periodic boundary conditions, a jump of the complex phase has to be introduced as a result of the chosen gauge of the vector potential (see [32]). Below, we present pictures of the evolution of the vortex distributions in time with a constant in-plane field while increasing the perpendicular field. Vortices are visualized as isosurfaces with constant order parameter $|\psi|$.

We will first briefly comment on the general picture of magnetization with crossing magnetic fields. Then we will describe in more detail the vortex cutting process. Finally, we will discuss the helical instability induced by the perpendicular field. Short movies of the vortex evolution can be found in the supplementary information.

Plate with surfaces parallel to the anisotropy axis -c ($\parallel Z$)

In this case, sample surfaces are parallel to the XZ-plane and the \mathbf{c} -axis is along Z. The initial field is along the X-axis, and the perpendicular field is parallel to Z. General changes of the vortex structure are illustrated in Fig.1, where we show the evolution of vortices without spatial disorder (“Clean”) in the left column and with weak disorder (“WD”) in the right column at the same values of time and field. $B_x = \text{const} = 0.04$ and B_z changes in steps of $\Delta B_z = 0.0005$ each $\Delta t = 3750\tau_{GL}$ from 0 to 0.0095 within the same time protocol for both Clean and WD cases. All visualizations of the internal vortex structure are done using isosurfaces of the order parameter amplitude, $|\psi| = 0.6$. There are no jump-wise changes in the vortex system due to the field steps and the structure does not become static between them. The vortex array dynamically adjusts to the steps on time scales larger than Δt , indicating the overdamped character of the vortex motion. To clearly present the arrangement of vortices we show three projections of the vortex arrays at each time and field.

Qualitatively, the evolution of the vortex state is very similar in both cases. In the initial state ($B_z = 0$) vortices are mostly aligned with the applied field (Fig.1a, a1). Vortices are smoothly bending in the XY-plane due to the introduced structural disorder, or thermal noise in the Clean case, but they do not bend along Z due to the anisotropy in the vortex line tension. They have elliptic cores extended perpendicular to the Z-axis as expected for the chosen anisotropy parameter. Close comparison at the same value of the order parameter shows that vortices are slightly wider in the WD case. There is a clear tendency towards the formation of a vortex lattice with a unit cell predominantly stretched along the Y-direction in accordance with predictions for anisotropic superconductors ((42) and refs. therein). This feature is clearly seen in z-projections of Fig.1 through the bunching of vortices dominating over their wiggling in the XY plane.

With increasing perpendicular field, B_z , vortices remain unchanged in the middle section while new tilted vortices, usually arched inside as shown by white arrow in Fig.1b, form at the XZ sample surfaces. They move preferentially perpendicular to the Z-axis and cross the inner vortices. After cutting and reconnection through an intricate process described below, the resulting vortices become tilted from the XY-plane. So the B_z

component is delivered from the surface by newly generated vortices and transferred to the initial vortices in the bulk through the cutting-reconnection events. The resulting tilted vortices aligned towards the external field lower the energy of the system (see scheme in Fig.2).

With increasing normal field, the resulting tilted vortices move inside together with new vortices arriving from the surfaces and the normal flux component steadily occupies the sample (Figs.1b-d, b1-d1). Interestingly, at the normal flux front there is a sharp change of the vortex angle. It is better observed in the illustration of the WD case in Fig.1b1 (see red arrow on X-projection, top-right panel). Here the left vertical stack of vortices is tilted by a noticeable angle compared to the inner vortices aligned mostly in the XY-plane. The difference in tilt is well resolved in the bottom Y-projection of Fig.1b1. A moving front of tilted flux penetration was observed experimentally in YBCO crystals under crossing fields (see [31] and refs there). Following Clem [43] one should expect that such fronts will carry enhanced currents responsible for the variation of the induction angle $d\theta/dr$ in contrast to Bean's vortex pinning currents limiting the transverse motion of vortices and defining the induction density gradients $d|\mathbf{B}|/dr$. At the largest $B_z=0.0095$, vortices tend to form chains, as predicted for tilted vortices in anisotropic superconductors [42].

The main difference between the Clean and WD case is an unexpectedly better mutual alignment of vortices in the disordered sample. Also, counterintuitively, at larger B_z vortices shift to a longer distance from the XZ sample surfaces in the presence of disorder (Fig.1d). Note, that the larger wiggling of vortices in the Clean case is mostly around the Z-axis while their tilt with respect to the Z-axis is nearly the same over the sample.

Plate with surfaces perpendicular to the anisotropy axis-c ($c||Z$)

Snapshots of the vortex structure evolution in the crossing fields for sample surfaces parallel to the XY plane are shown in Fig.3 for both Clean (left column) and WD (right column) cases. They are calculated within the same time-field protocol as discussed above and presented with the same t and B_z values as in Fig.1. The emerging vortex configurations are qualitatively similar to those in the sample with XZ-surfaces. However, now vortices arrange more irregularly across the Z-axis and do not show a tendency to form a regular lattice. This can probably be associated with increased interactions of vortices with sample surfaces perpendicular to the anisotropy axis, which interferes with interactions between vortices defining their order. Although vortex-vortex coupling remains still dominating and at larger tilt angles results in a set of distorted vortex chains (see vortex stacks vaguely aligned in YZ planes marked by arrows on X-projection of Fig.3d). Differences between the Clean and WD cases are much less noticeable. A new feature in Fig. 3 compared to Fig. 1 (see Y-projections in b-d panels and top-right insert) is a noticeable tilt of the vortex ends near the XY-surfaces. This is an expected effect (see e.g. [44]) of the supercurrents flowing preferentially in the XY-plane near the surface and aligning these vortices towards the Z-axis.

Vortex loops penetrating from the XZ surfaces and crossing-reconnecting with initial vortices produce new tilted vortices in the bulk. The tilted vortices move further inside, forming a front, which is less pronounced than in the sample with XZ-surfaces. Near the front, we observe helical instability (see the last section), also resulting in tilted vortices.

For the maximum B_z (Fig. **3d, d1**), tilted vortices are assembled closer to the center of the sample than in Fig. **1**. We do not observe the entry of new vortices from the XY-surfaces but they always propagate from the XZ-edges of the simulation volume. This can be referred to the advanced mobility of anisotropic vortices in the direction across the Z-axis.

Vortex crossing

As pointed out above, the main phenomenon resulting in the tilt of flux lines in the bulk is cutting and reconnection of vortices followed by their straightening in a new direction. To study details of the cutting, we first identified crossing events with time steps of τ_{GL} and then decreased the time steps to $0.1\tau_{GL}$ within the event duration. This allowed us to reveal characteristic features of the process and follow the dynamics using reasonable calculation efforts. For all studied geometries and both Clean and WD cases the process was very similar and below we illustrate it with a couple of characteristic pictures.

Fig. **4** presents typical consecutive stages of the cutting and reconnection of two vortices on a large time scale. Two different projections (with shown coordinate axes) of the same event are visualized in the top two and bottom two rows. The moving vortex loop entering from the edge at increasing B_z is green and the initial vortex, generated by the longitudinal field B_x , is yellow.

As the two vortices approach each other, they mutually bend to acquire a local antiparallel orientation (Fig. **4a, a1**). The local bending of vortices increases their length and their elastic energy but strongly reduces their repulsion energy, ultimately resulting in their local attraction. The more mobile entering vortex (generated by the increasing perpendicular field B_z) usually bends more than the initial vortex (created by the parallel field B_x). The cores of two vortices touch (Fig. **4b, b1**) and merge locally (Fig. **4c, c1**). Then the merged core segment deforms (Fig. **4d, d1**) and breaks resulting in a pair of new highly twisted vortices consisting of exchanged halves of the initial vortices (Fig. **4e, e1**). The peculiar strong twist (marked by arrow in Fig. 4e1) of vortices around the Z-axis is a consequence of the superconducting anisotropy leading to much smaller line tension in the XY-plane [23]. Eventually, strong twists of the departing vortices stretch out, resulting in a pair of tilted vortices (Fig. **4f, f1**).

The second example, Fig. **5**, illustrates the crossing of an initial linear vortex with an expanding helical vortex (details of the helical instability are discussed later). The main features are the same as in the previous case but the helical vortex is already in a twisted configuration before it approaches the linear vortex (Fig. **5a, a1**). When the vortices are close, the linear vortex also starts to bend and the twist on the helix becomes more pronounced (Fig. **5b, b1**). Subsequently, the vortex cores merge (Fig. **5c, c1**) and then deform and split forming two different vortices with exchanged halves. These new vortices produced by cutting-reconnection depart (Fig. **5d, d1**) and later straighten (not shown), resulting in a pair of vortices tilted towards the field direction.

To follow the dynamics of the vortex cutting process we calculated the time dependence of the minimum distance (r_{min}) between centerlines of mutually bent vortices. The position of the centerlines was found using closed contour integration of the gradient of

phase of the complex order parameter over the mesh faces, and choosing subsets which produce 2π phase shift within (see [45]). Subsequent triangulation and tracing of the center point then yield the vortex line with a sub-grid resolution. Remarkably, this procedure reveals the centerlines even when vortex cores are already well merged. Fig. 6 shows a set of $r_{\min}(t)$ dependences for a number of crossing events. Here, the time coordinate for each event is shifted so that the moment of collapse corresponds to $t=0$. The events are taken at different real time and B_z values at different points in the sample. In spite of all that, they show practically the same time duration of the crossing process. First, vortices approach with relatively low velocity (negative times on the plot). Then, at small distances (separations), they accelerate (at $t \rightarrow 0$). At this stage they experience a strong mutual twist. Finally, after the collapse (the exact position $r_{\min}=0$ is not resolvable in our simulations) they first depart with high velocity and then decelerate to a lower speed. The difference in separation, across which the approach and departure of the crossing event occurs, is not surprising because the events take place in different neighboring vortex environment and at different B_z . Interestingly, these factors do not change the average duration of the events, which is also independent of the presence of the weak spatial disorder. However, we believe that the introduction of strong pinning should introduce noticeable changes in the dynamics of the vortex cutting due to the pinning of the bent vortex segments.

Our numerical calculations of the total Ginzburg-Landau energy, E_{GL} , in the volume surrounding the vortex collision point show that during the crossing process, E_{GL} drops and then increases again. The value of the E_{GL} drop yields an estimate of the crossing barrier as $E_{cr} \sim 10.5 T_c$. From the simulated vortex behavior, such a barrier is not a serious obstacle for the cutting-reconnection process in our case. At the same time, such a considerable E_{cr} leaves the possibility of vortex entanglement under different conditions (orientation and magnitude of the field and presence of stronger pinning centers).

Left-handed helical vortices

The helical deformation of straight initial vortices is an independent and simultaneous process that emerges during the application of a perpendicular field. It also leads to vortex crossing and results in the orientation of vortices along the new field direction. A model of the helical vortex instability accompanied by flux-cutting was introduced by Clem [29] to explain the behavior of current carrying superconducting wires in longitudinal field. The self-field of the current I is circular (azimuthal) at the surface of the wire and couples to the applied longitudinal field H to generate clock-wise twisted (right-handed) helical vortices at large enough I and H . The Lorentz force of the current squeezes these helices towards the wire axis, where they become parallel to H , resulting in a process akin to longitudinal field pumping. Experimentally, such pumping was never observed and instead, inhomogeneous oscillations of the voltage along the wire were detected [46]. Clem suggested [29] that counter-clockwise twisted helices (left-handed) nucleate from the straight vortex lines in the middle of the wire and naturally expand towards the periphery of the wire due to the Lorentz force of the same current (Fig. 7). These left-handed helices collapse when they come in contact with the inward propagating right-handed helices, preventing parallel field pumping and resulting in voltage oscillations.

Brandt [30] showed that a similar helical instability should occur in the vortex lattice in the presence of currents flowing parallel to vortices. Later, Genenko analyzed the

appearance of helical vortices in different samples accounting for the effect of surface barrier on vortex entry [47]. So far, the experimental efforts to confirm the above theoretical predictions of nucleation and collapse of the helical vortices are mostly limited to macroscopic measurements as discussed in [48, 19].

In our simulations, the appearance of helical vortices with increasing B_z can be seen in the large-scale pictures of Fig. 1c and 3c (see top-right X-projections). A more detailed illustration is presented in Fig. 8. Here, we show by arrows the direction of both B_x and B_z along with the screening B_z currents J_c . Circles with arrows around the current lines indicate the chirality of the expected right-handed vortices that would be supported by these currents. Our simulations reveal vortex helices that are all left-handed, following Clem's predictions. The resulting Lorentz force $\mathbf{F}_L = \mathbf{J}_c \times \Phi_0$, where Φ_0 defines locally oriented helical vortex flux, is directed outwards from the helix axis and thus should expand the left-handed helix in accordance with our simulations. The expanding helices cross and reconnect with the initial vortices introduced by B_x , as e.g. shown in Fig. 5, and produce new tilted vortices. Segments of helices that are tilted opposite to the applied B_z expand towards the XZ-sides and exit the sample.

Results of the simulations shown in Fig. 8 correspond to the plate perpendicular to the Z-axis i.e. normal to B_z . However, very similar left-handed helices appear in the plate parallel to the Z-axis. The spatial disorder also does not introduce any noticeable changes in this picture. Due to the anisotropy, helical vortices expand preferentially perpendicular to the Z-axis (Fig. 9) and outline a flat cylinder extended along the XY-direction as schematically shown Fig. 9d. Thus, helical instability is a universal component of the crossing-field magnetization process with some geometrical distortions introduced by the superconducting anisotropy.

Conclusions

In this work we used time dependent Ginzburg-Landau model to simulate the vortex cutting and reconnection process under applied crossed magnetic fields. Using massive parallel simulations on GPUs, we managed to follow the behavior of a relatively large array of vortices with high time resolution of $0.1 \tau_{GL}$ in anisotropic high- T_c superconductor, accounting for weak disorder, thermal noise, and specific geometry of the sample.

The vortex cutting process emerges when longitudinal magnetic field induced vortices in a superconductor intersect with incoming orthogonal vortices induced by an applied perpendicular field. Two approaching vortices bend to form local twists near the crossing point to arrive at a locally antiparallel configuration. Their vortex cores merge and then deform and break-away locally, leaving two new vortices consisting of the exchanged halves of the initial vortex lines with strong local twists. Eventually, the twisted sections straighten out and the resulting vortices end up tilted towards the direction of the applied magnetic field. The simulated time-lapse images of the cutting process reveal the acceleration of the vortex as it approaches the crossing point and a deceleration of the newly cut and reconnected vortices as they retreat from each other. We believe that the introduction of strong pinning can substantially delay vortices in the close vicinity of the crossing point due to the trapping of strongly bent segments at the pinning centers.

The entry of the tilted flux from the surface is accompanied by a helical deformation of longitudinal vortices induced by currents that screen the perpendicular field and are

parallel to the vortices,. These helical vortices are left-handed in accordance with the predictions by Clem [29]. They expand under the Lorentz force of the same screening current and cut-reconnect with initial straight vortices, resulting in tilted flux lines. We find that both the expansion of helices and the cutting-reconnection of vortices are noticeably modified by anisotropy.

Our study of the vortex cutting phenomenon yield crossing patterns that are very similar to those observed in hydrodynamic stimulations of the reconnection process of vortices in classical and quantum liquids [49, 50, 17]. This similarity is not accidental. In fact, in the case of quantum liquids the dynamic Gross-Pitaevskii equation (see e.g. [51]) has nearly the same form as TGDL,. In usual liquids the similarity is not that obvious and points to a qualitative analogy between transformations in the viscous flow and in the electric current variations in superconductors. It hints at the possibility of a coarse-grain hydrodynamic approach to describe the current and magnetic flux dynamics in superconductors.

Our results is a first step towards a fundamental understanding of ‘bulk’ vortex crossing phenomena in superconductors. Further studies of vortex crossing should address different scenarios for vortex cutting, characteristic times of the event, accurate statistical estimates of the crossing barrier, and topological changes in the current patterns around the crossing points. Answers to these questions should depend on the material parameters defining the shape, coupling efficiency, and cutting barrier of intersecting vortices, such as anisotropy, sample geometry, layered crystal structure, and different pinning landscapes. This opens a vast field for exploration that can be extended to many vortex phenomena in other physical systems. We hope our results will attract wide attention to this exciting problem, which can be approached using comprehensive TDGL simulations.

ACKNOWLEDGMENTS This work was supported by the U.S. Department of Energy, Office of Science, Materials Sciences and Engineering Division, and Office of Advanced Scientific Computing Research, Scientific Discovery through Advanced Computing (SciDAC) program.

References

- [1] M. Faraday, *LVIII. On the Physical Character of the Lines of Magnetic Force*, Philosophical Magazine and Journal of Science, p.402-428 (1852).
- [2] A. A. Abrikosov, *Sov. Phys. JETP* **5**, 1174 (1957).
- [3] A. Kanda, B. J. Baelus, F. M. Peeters, K. Kadowaki, Y. Ootuka, *Phys. Rev. Lett.* **93**, 257002 (2004).
- [4] I. Lukyanchuk, V. M. Vinokur, A. Rydh, R. Xie, M. V. Milosevic, U. Welp, M. Zach, Z. L. Xiao, G. W. Crabtree, S. J. Bending, F. M. Peeters, W.-K. Kwok, *Nat. Phys.* **11**, 21 (2015).
- [5] A. P. Malozemoff, *MRS Bull.* **36**, 601 (2011).
- [6] J. W. Bray, *IEEE Trans. Appl. Supercond.* **19**, 2533 (2009).
- [7] S. K. Remillard, S. Cordone, *J. Supercond. Novel Magn.* **19**, 523 (2009).

- [8] V. K. Kaplunenko, A. V. Ustinov, Eur. Phys. Journ. B **38**, 3 (2004).
- [9] M. H. Devoret, R. J. Schoelkopf, Science **339**, 1169 (2013).
- [10] D. R. Nelson, H. S. Seun, Phys. Rev. B **39**, 9153 (1989).
- [11] A. Schonenberger, V. Geshkenbein, G. Blatter, Phys. Rev. Lett. **75**, 1380 (1995).
- [12] M. J. W. Dodgson, M. A. Moore, Phys. Rev. B **51**, 11887 (1995).
- [13] D. Ertas, D. R. Nelson, Physica C **272**, 79 (1996).
- [14] G. P. Bewley, M. S. Paoletti, K. R. Sreenivasan, D. P. Lathrop, Proc. Natl. Acad. Sci. U.S.A. **105**, 13707 (2008) .
- [15] M. S. Paoletti, D. P. Lathrop, Ann. Rev. Cond. Mat. Phys. **2**, 213 (2011).
- [16] M. W. Scheeler, D. Kleckner, D. Proment, G. L. Kindlmann, W. T. M. Irvine, Proc. Natl. Acad. Sci. U.S.A. **111**, 15350 (2014).
- [17] C. E. Laing, R. L. Ricca, D. W. L. Sumners, Sci. Rep. **5**, 1 (2015).
- [18] E. H. Brandt, J. R. Clem, D. G. Walmsley, J. Low. Temp. Phys. **37**, 43 (1979).
- [19] A. M. Campbell, Supercond. Sci. Technol. **24**, 091001 (2011).
- [20] E. H. Brandt, U. Essmann, Phys. Stat. Sol. B **144**, 13 (1987).
- [21] E. H. Brandt, M. P. Das, J. Supercond. Nov. Magn. **24**, 57 (2011).
- [22] P. Wagenleithner, J. Low Temp. Phys. **48**, 25 (1982).
- [23] A. Sudbo, E. H. Brandt, Phys. Rev. Lett. **67**, 3176 (1991).
- [24] C. Carraro, D. S. Fisher, Phys. Rev. B **51**, 534 (1995).
- [25] M. A. Moore, N. K. Wilkin, Phys. Rev. B **50**, 10294 (1994).
- [26] M. Machida, H. Kabaraki, Phys. Rev. Lett. **71**, 3206 (1993).
- [27] E. Sardella, P. N. L. Filho, C. C. de Souza Silva, L. R. E. Cabral, W. A. Ortiz, Phys. Rev. B **80**, 012506 (2009).
- [28] M. Bou-Diab, M. J. W. Dodgson, G. Blatter, Phys. Rev. Lett. **86**, 5132 (2001).

- [29] J. R. Clem, Phys. Rev. Lett. **38**, 1425 (1977).
- [30] E. H. Brandt, J. Low Temp. Phys. **44**, 33 (1981); J. Low Temp. Phys. **44**, 59 (1981).
- [31] V. Vlasko-Vlasov, A. Koshelev, A. Glatz, C. Phillips, U. Welp, W. Kwok, Phys. Rev. B **91**, 014516 (2015).
- [32] I. A. Sadovskyy, A. E. Koshelev, C. L. Phillips, D. A. Karpeyev, A. Glatz, J. Comput. Phys. **294**, 639 (2015).
- [33] A. Schmid, Phys. Kondens. Mater. **5**, 302 (1966).
- [34] L. P. Gor'kov, G. M. Eliashberg, Sov. Phys. JETP **27**, 328 (1968).
- [35] N. B. Kopnin, *Theory of Nonequilibrium Superconductivity*, Oxford Univ. Press, Clarendon Press, 328 pp. (2001).
- [36] I. S. Aranson, L. Kramer, Rev. Mod. Phys. **74**, 99 (2002).
- [37] M. Ogren, M. P. Sorensen, N. F. Pedersen, Physica C **479**, 157 (2012).
- [38] K. S. Grishakov, P. N. Degtyarenko, N. N. Degtyarenko, V. F. Elesin, V. S. Kruglov, Physics Procedia **36**, 1206 (2012).
- [39] G. R. Berdiyrov, M. M. Doria, A. R. de C. Romaguera, M. V. Milosevic, E. H. Brandt, F. M. Peeters, Phys. Rev. B **87**, 184508 (2013).
- [40] L. Peng, Z. Wei, Y. Liu, Y. Fang, C. Cai, J. Supercond. Nov. Magn. **27**, 1217 (2014).
- [41] G. Carapella, P. Sabatino, M. Gombos, Physica C **515**, 7 (2015).
- [42] S. J. Bending, M. J. W. Dodgson, J. Phys. Cond. Mat. **17**: R955 (2005).
- [43] J. R. Clem, Phys. Rev. B **26**, 2463 (1982).
- [44] E. H. Brandt, Phys. Rev. B **48**, 6699 (1993).
- [45] C. L. Phillips, T. Peterka, D. Karpeyev, A. Glatz, Phys. Rev. E **91**: 023311 (2015).
- [46] A. M. Campbell, J. E. Evetts, Adv. Phys. **21**, 199 (1972).
- [47] Yu. A. Genenko, Phys. Rev. B **51**, 3686 (1993); Phys. Rev. B **53**, 11757 (1996).
- [48] J. R. Clem, Phys. Rev. B **83**, 214511 (2011).
- [49] S. Kida, M. Takaoka, *Vortex reconnection*, Ann. Rev. Fluid Mech. **26**, 169 (1994).

[50] J. Koplik, H. Levine, *Vortex Reconnection in Superfluid Helium*, Phys. Rev. Lett. **71**, 1375 (1993).

[51] S. Zuccher, M. Caliari, A. W. Baggaley, C. F. Barenghi, Phys. Fluids **24**,125108 (2012).

Figure Captions

Fig.1 Snapshots of the vortex configurations during application of the perpendicular field (B_z) to the sample with initial vortices formed in the longitudinal field ($B_x= 0.04, B_y=0$). Boundary conditions imitate a plate with XZ-surfaces parallel to the anisotropy axis $\mathbf{c} \parallel Z$ (shaded planes in the top insert) . Appropriate time values t (in units of τ_{GL}) and B_z (in units of H_{c2}) are shown near the panels. Three projections along Z- (left), X-(right-top), and Y-axis (right-bottom), are shown for each t - B_z pair. Left column (a-d) presents data for the Clean case (no spatial disorder) and the right column (a1-d1) shows data at the same t - B_z in the case with disorder (WD). Vortices are visualized by isosurfaces of the order parameter $|\psi|=0.6$.

Fig.2 Simplified scheme of the vortex rotation in the bulk through the cutting-reconnection process. (a-b) New vortex, N, delivers the normal field component ($H_{\perp} \parallel Z$) from the surface to the initial vortex, I, generated in the in-plane field $H_{\parallel} \parallel X$. After crossing (b), new reconnected vortices stretch due to the vortex line tension and become tilted towards the applied field direction (c).

Fig.3 Same as in Fig.1 but for boundary conditions imitating a plate with XY-surfaces (shaded planes in the top-left sketch) perpendicular to the anisotropy axis $\mathbf{c} \parallel Z$. Top-right insert illustrates the tilt and expansion of vortices near the XY sample surface.

Fig.4 Close-up of the vortex crossing process in Clean plate with XY-surfaces perpendicular to the anisotropy axis \mathbf{c} . $\mathbf{B}=(0.04, 0, 0.0025)$. Time values in units of τ_{GL} are shown on the (a-f) panels. Initial vortex is yellow, new entering vortex is green. Bottom panels (a1-f1) show the same crossing stages in slightly tilted projection.

Fig.5 Crossing of the expanding helical vortex (green) and the initial straight vortex (yellow). Time values are shown in (a-d). (a1-d1) panels show the same stages in different projection. $B_x=0.04, B_z=0.006$. Clean case, plate with surfaces perpendicular to the \mathbf{c} -axis.

Fig.6 Time dependence of the minimum distance between vortex centerlines, r_{min} , for several crossing events. Individual crossing events are taken at different time and B_z values, in different parts of the sample and with different arrangement of neighboring vortices, which causes varying initial and final r_{min} . However, the time evolution of the process looks the same. Time coordinates for different events are adjusted so that $t_a=0$ corresponds to the

collapse moment. r_{\min} is in units of ξ_0 and t_a in τ_{GL} . Note, that our procedure of tracing the centerlines of vortices yields a sub-grid resolution and a smoothed trajectory of the vortex core motion.

Fig.7 Helical deformations of vortices parallel to the magnetic field \mathbf{H} at strong longitudinal currents J (in accordance with (29-30)). Lorentz force (small arrows) on the clockwise twisted (right-handed, RH) vortices should squeeze them into a straight line, but it should expand counterclockwise twisted (left-handed, LH) vortices.

Fig.8 Development of the helical instability at increasing B_z observed in the simulations. Helices at the left and right sides have opposite chirality, but they are all left-handed with respect to the screening currents J_c . $t=57250$, $B_x=0.04$, $B_z=0.0065$. Clean plate perpendicular to the \mathbf{c} -axis. Similar patterns appear in the plate parallel to the \mathbf{c} -axis.

Fig.9 (a-c) Three projections of the helical vortex near the right side of the sample illustrated in Fig.8 (Clean plate with surfaces perpendicular to the \mathbf{c} -axis, $t=57500$, $B_x=0.04$, $B_z=0.0065$). (d) The scheme of the elliptical trajectory of helix in the anisotropic material. (e) Front of helices formed near the left side of the sample illustrated in Fig.1 (Clean plate parallel to \mathbf{c} , $t=73250$, $B_z=0.0085$).

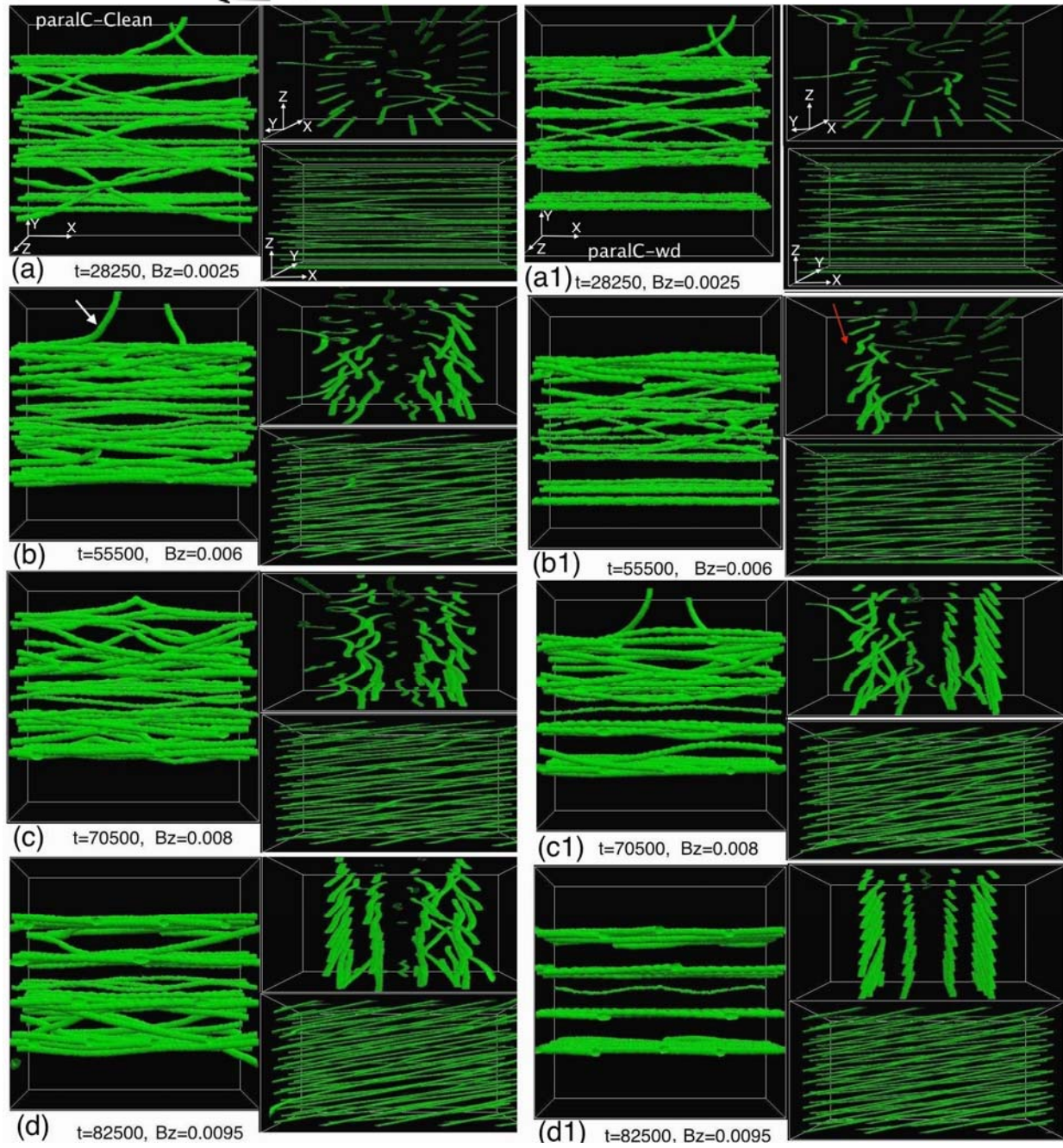
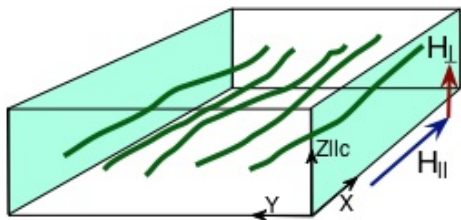


Fig.1

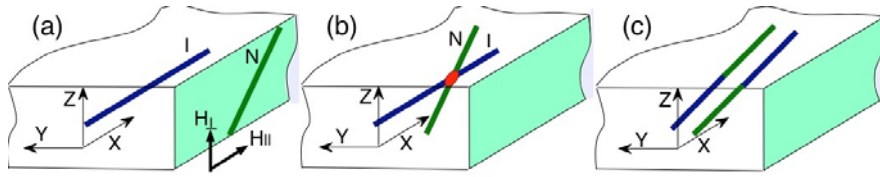


Fig.2

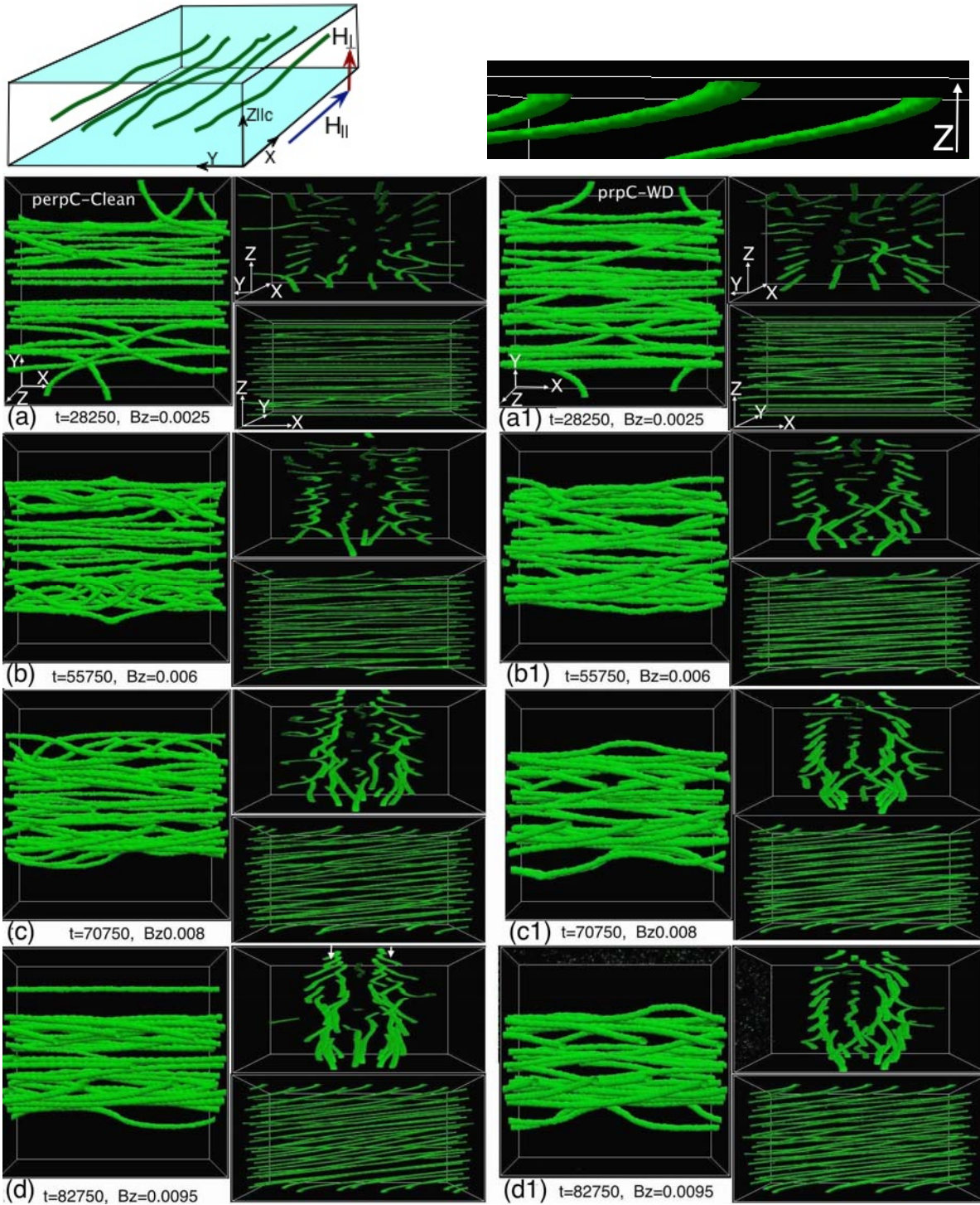


Fig.3

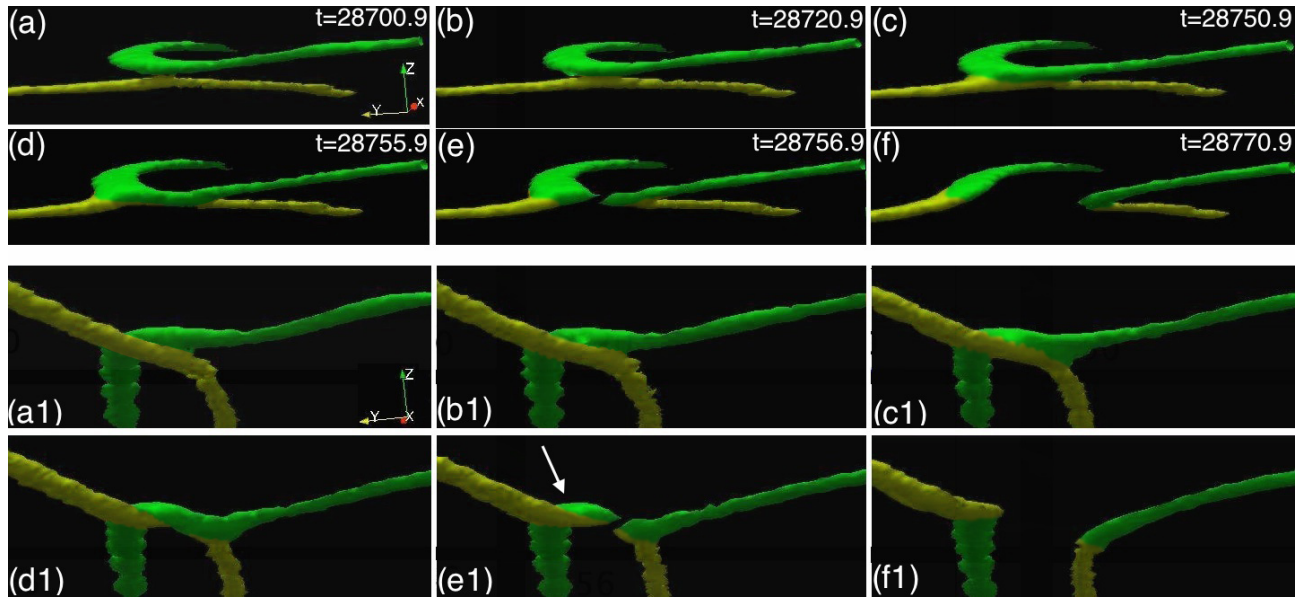


Fig.4

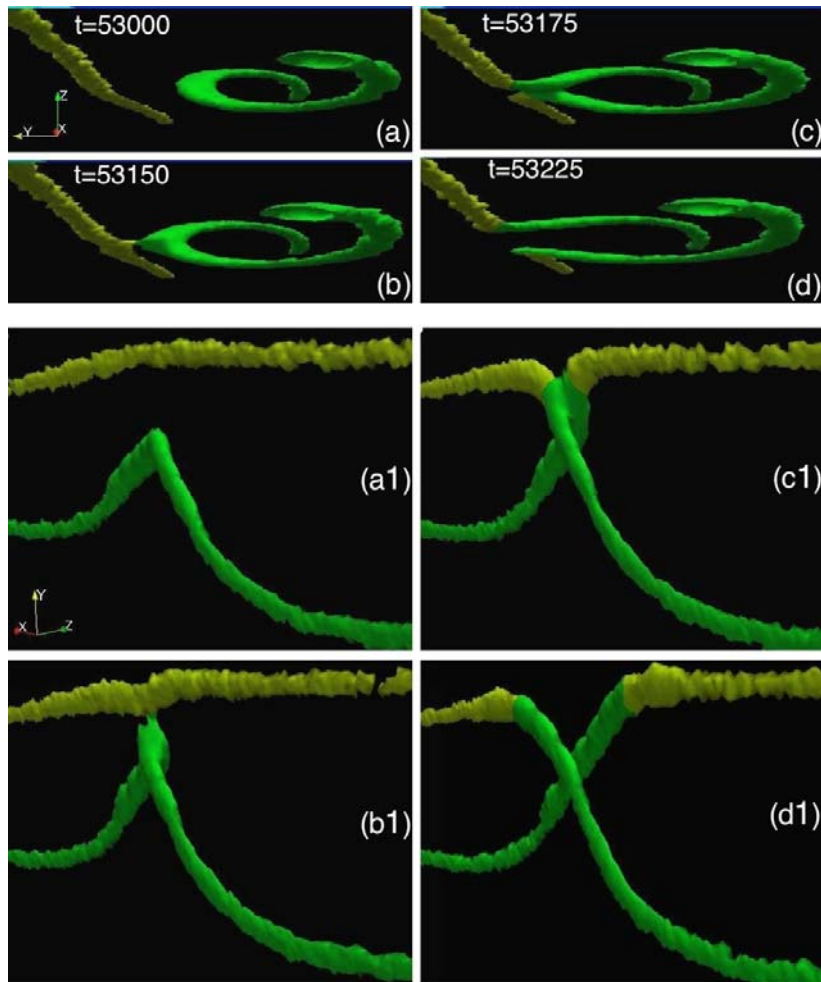


Fig.5

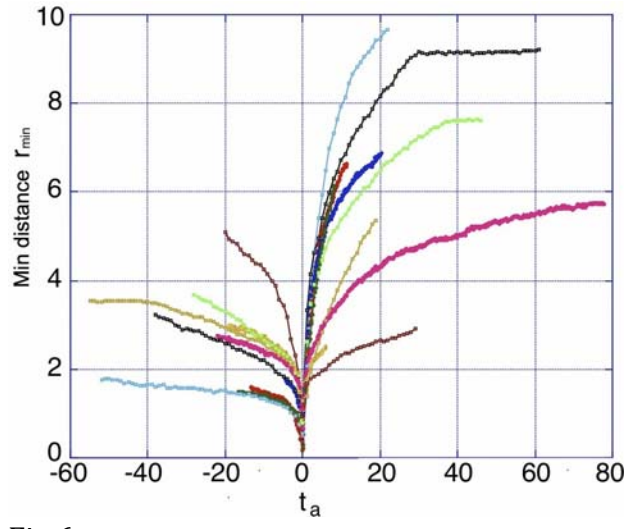


Fig.6

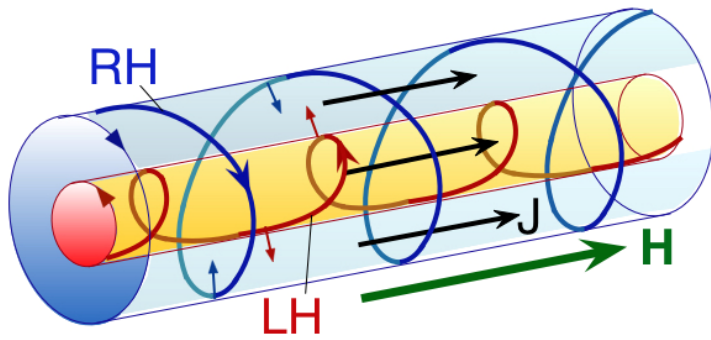


Fig.7

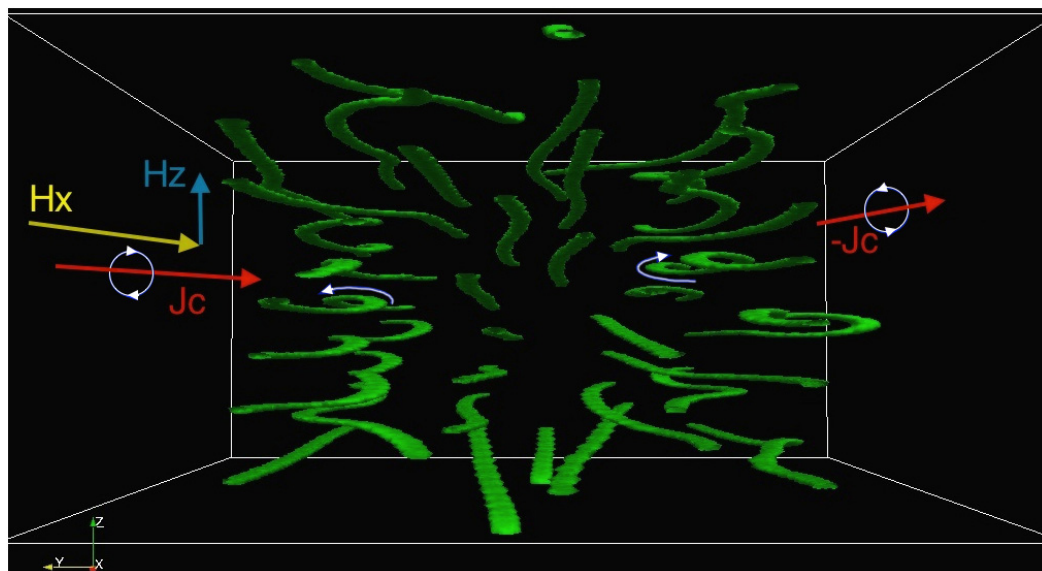


Fig.8

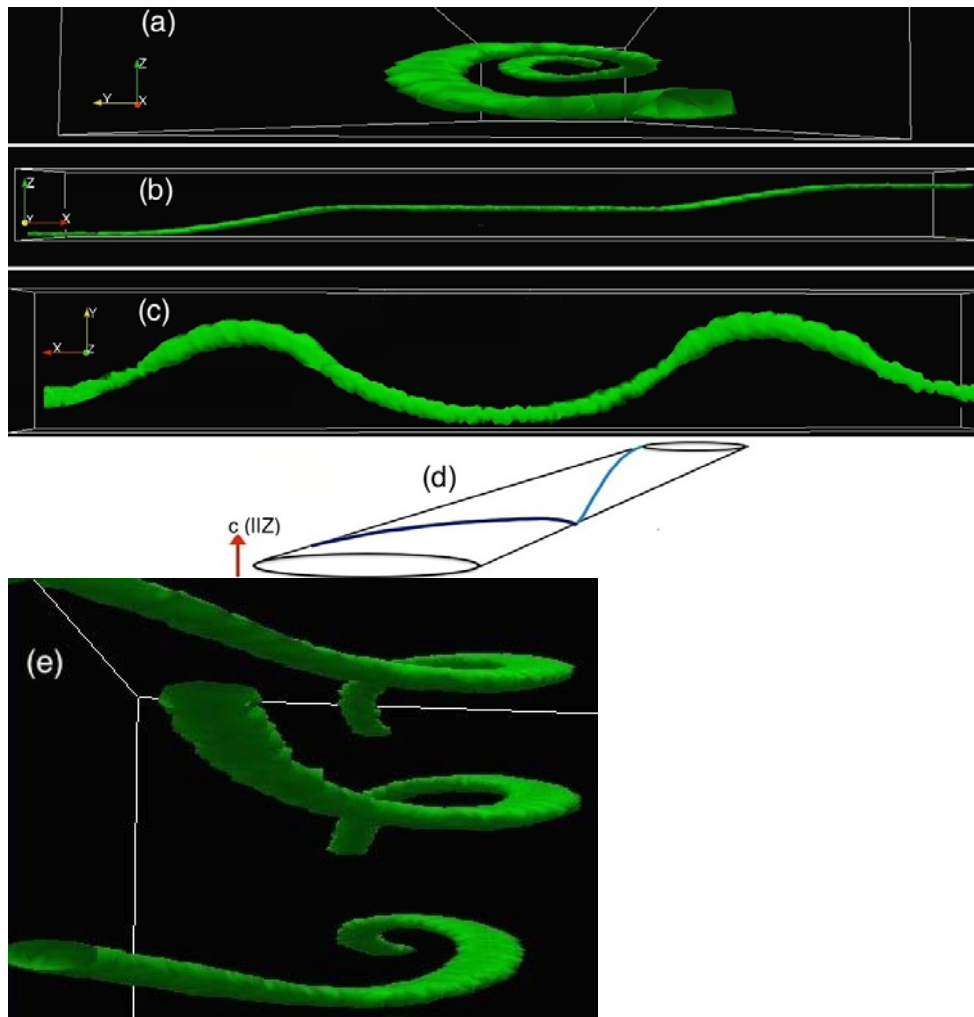


Fig.9